ρ_f

Strengthened infilled RC Frames: Continuum and Macro modeling in nonlinear finite element analysis

Breveglieri M., Camata G., Spacone E.
Geology and Engineering Department - University "G. D'Annunzio" Chieti-Pescara, Italy

Abstract

Strengthening and retrofitting masonry infill Reinforced Concrete (RC) frames is a crucial topic, due to the large use of this structural typology in earthquake affected countries. Masonry infills can provide a positive and negative effect on the seismic response. Positive, because the infills dissipate energy and therefore increase the overall damping, negative because if their disposition is irregular or they fail irregularly the structure behavior becomes irregular, in addition they stiffen the structure and thus increase the base shear force. However, it has been shown that by using an adequate strengthening technique, performance and safety of the structures and of the infills can be improved. Several models for Un-Reinforced Masonry (URM) infills have been developed in the past, but there is a lack of models available to describe the behavior of strengthened infilled frames

An analytical simplified strut and tie model is proposed based on the results obtained with the FE analyses. In the simplified model the tensile tie and compression strut depend on the stiffness and strength of the reinforcement in addition to the geometrical and mechanical parameters. Lateral stiffness and strength obtained with this model show a good agreement with the tests and the continuum FE models. .

The model is validated with experimental results of Carbon Fiber Reinforced Polymer (CFRP) strengthened infilled RC frame. The experimental data are studied by means of continuum Finite Element (FE) models in order to study the influence of various parameters on the seismic response and to calibrate the simplified model.

1. Introduction

Masonry infilled RC frames have been widely studied in order to understand the interaction between the RC frame and the masonry infill subjected to lateral forces and seismic action. This type of construction is largely used in seismic areas around the world. Design applications range from single two-floor family dwellings to high-rise apartment buildings in countries such as Chile, Canada, Mexico, Peru, Turkey, India, Nepal and China [1]. These types of buildings can also be found in the south Mediterranean area in countries affected by earthquakes, like Algeria, Italy, Spain, Portugal, Greece, and Turkey. Their widespread presence has serious social and economic implications. Recent earthquakes in Mediterranean areas such as Turkey (Erzincan, Düzce and İzmit 1999), Italy (L'Aquila 2009, Emilia 2012, Central Italy 2016), Nepal (2015) and China (ichuan, 2008), have shown the importance of masonry infilled frame on the structural behavior of mid-rise RC frame buildings.

Researchers agree on the interaction mechanism; experimental test and earthquake events have demonstrated that for relatively small lateral displacement a diagonal truss action in the infill is generated. The formation of a masonry compression strut introduces a concentrated force acting on the frame corners, with the separation of the infill from the frame on the opposite side. This mechanism can induce significant damage in the RC structural elements as well as the failure of the masonry infill and different failure modes of the structural system [2–4]. The overall stiffness of the building increases, its fundamental frequency increases, and as a consequence the base shear force increases due to seismic action. In addition, irregular infill disposition or irregular failures could trigger an irregular structural behavior. Therefore, the infill-frame interaction should be considered to model the seismic behavior. Most seismic design codes, including Eurocode 8 [5], introduce some penalty factor for irregularities in plan or elevation, but they do not suggest any procedure to calculate the lateral stiffness and resistance of the infills [6,7]. Strong infill walls in weak or even ductile RC frame may affect the response of frames by seriously damaging the RC element and leading to the collapse of the structure [1,8,9]. In this case, it can be beneficial to isolate the infills from the structure with soft joints and secure the wall against out-

of-plane actions [10]. In this way the infills can be modeled as mass without stiffness (as indicated for new construction in [11]. This solution guarantees that there is no damage in the infills, however it generates other problems for the building energy efficiency and an external cappotto needs to be added to the building. If masonry infills are regularly placed within the structure and do not trigger shear failures in the columns, they could have a beneficial effect on the structural response [12–19]. The infills carry part of the seismic action, consequently relieving the structural system, and extensively increase the ability of the building to dissipate energy [20]. In moderate earthquakes and especially in the case of existing RC frame buildings, typically lacking in stiffness and strength, the masonry infill can be considered as a fundamental element in an intervention of seismic retrofitting. The FEMA 306, for example, provides a simple and conservative formulation in order to consider the masonry infill behavior. In order to increase the performance of the infill, mainly by increasing the ductility of the system, a positive effect was highlighted by the shear connector between concrete and masonry [21]. However, to ensure greater efficiency intervening in the structural system by strengthening both frame and the masonry and converting the non-load bearing existing masonry wall into a structural system is recommended.

In the last decades it has been demonstrated that for this strengthening or retrofitting intervention different types of materials and techniques can be successfully used. As an alternative to thick overlays of concrete reinforced plaster [22] and shotcrete with metallic mesh, which substantially increase the structure weight and stiffness, more recent and modern lighter materials have been proposed to improve the infilled frame performance.

Most of the tests have been carried out using Fiber Reinforced Polymer (FRP) as strengthening material [23–32] and interesting results have recently been presented by applying Textile reinforced Mortar/Fabric Reinforced Cementitious Matrix (TRM/FCRM) [33], Engineered Cementitious Composite (ECC) [34,35]. In general, all these strengthening/retrofitting solutions have impacted the strength of the system,

the ability to dissipate energy and showed higher ductility at ultimate displacement. This type of intervention besides the main objective which is the "in plane strengthening", improve the out of plane behavior also when small percentages of material are used. A key factor in the strengthening effectiveness highlighted during the experimental test has been the connection methodology between the frame and the masonry infills. Other structural /retrofitting approaches consist of removing the existing masonry infills and replacing them with a new structural system properly designed with dissipative and resisting properties (i.e. additional steel bracing and dampers). The advantage of this strategy lies in the possibility to have a better understanding of a properly engineered "infill substitute." Nevertheless this solution could be economically not viable.

Several experimental tests have been produced in order to understand and verify the effectiveness of strengthened and retrofitted masonry infilled RC frames, but there is a lack of analytical models able to correctly predict the structural behavior of the strengthened masonry and its interaction with the RC frame. This step is fundamental, to widely employ these techniques and extend their use to a multi-story building.

This paper aims to introduce a macro model in order to include the strengthening contribution, by varying the strengthening geometry or the strengthening percentage. The study is carried out by analyzing masonry strengthened RC frames tested by Yuksel et al. [27], for which the strengthening strategy was represented by diagonal CFRP extended to the RC frames and anchored to the masonry with textile anchors. The numerical and analytical behavior of strengthened masonry infilled frame is studied here using two different modeling techniques. The first consist of continuum modeling. By following this approach the experimental results are reproduced at the mesoscale. The second consists of a macro-modelling approach, which idealizes the strengthened masonry infill as a strut and tie system. By following this approach the generated analytical model to describe the strengthened masonry can be easily extended to multistory structures.

2. Methodology

2.1 Modeling approaches

The choice of the numerical modeling strategy has to be targeted to specific needs and it depends on the scale of the investigation. To model the infills three approaches are used: micro-modelling, continuum modeling, and macro-modelling [3]. The first approach considers the detailed micro-modelling and the simplified micro-modelling. Bricks and mortar joints (for detailed micro-modelling) are discretized using continuum elements, while discontinuous elements are used to represent the behaviors of the mortar joints and brick-mortar interfaces. By adopting this approach the mortar failure and separation between bricks can be observed. In the continuum approach, the infill panel is modelled as a homogeneous material and the cracking is smeared. Contact, gap or spring elements can be added to the model to consider the interface infill-frame to allow separation of the infill from the bare frame. The macro-modelling approach uses 1D elements, the infills are modelled with equivalent struts and the RC frame with beam elements. This approach, faster and easier to apply using commercial codes, is of greater interest for designers and engineers. For the first two approaches, the frame can be modeled considering the concrete and steel reinforcement as different elements; while in the last approach the reinforced concrete elements are modeled with beam elements using lumped plasticity or using distributed fiber models. Further information on the numerical modeling of masonry infilled frame can be found in [2,3,36,37]. As for the masonry infilled frame, all models can predict the structural behavior in terms of static, cyclic, and dynamic loading, however only the first two can evaluate local effects. Nevertheless, as shown in the published literature, the micro modeling requires a complete material characterization and calibration of several parameters and difficulties can arise due to convergence.

In this paper, the experimental tests carried out by Yuksel et al. [27] are analyzed, by adopting continuum and macro modeling approaches. The continuum model is used to investigate details on the failure

mechanisms and interaction effects between infill and frame. The proposed numerical method can reproduce the static behavior of the specimen at global and local level with and without strengthening. The numerical results are used for the analytical calibration of the macro model.

In the proposed study on strengthened infills a tensile tie is added to the compression diagonal strut to simulate the effect of the CFRP [38]. Moreover, CFRP strengthening increases the compression strut width, as shown by the experimental and numerical evidence, and thus the geometry of the compression strut is adapted taking into account the modified stiffness of the infill.

2.2 Subject of the study

This study analyses the static and cyclic behavior of infilled RC frames strengthened using FRP materials and focuses on the experimental program on 1/3-scaled RC frames tested in Yuksel et al. [27], specimens' geometry and internal reinforcement are shown in Fig.1. The original design represented typical existing Turkish RC frames, characterized by lack of confinement in beam-column joints, minimal percentage of stirrups and low concrete compressive strength, 19 MPa was used in the experimental campaign. The longitudinal reinforcement ratios in columns and beams were taken as 1% and the transverse reinforcement ratio was taken as 0.4%. The steel reinforcement had yielding and ultimate stress of 420 MPa and 500 MPa, respectively. The masonry infill was made up of 1/3 scale clay brick, 88x84 x57 mm [39], with 41% percentage of voids. A cement based material has been used as mortar and as plaster. The wall thickness was around 70 mm including the lateral plaster thickness.

The masonry compressive strength was characterized by masonry wallet (500x500) compression test, whose results, gave a compressive strength of 4.85 MPa along the direction parallel to the holes and 3.43 MPa along the direction perpendicular to the holes [39]. A diagonal compression test was carried out to determine the tensile strength of the masonry, which resulted to be 0.92 MPa. Several types of strengthening configuration under unidirectional cyclic loading up to a drift ratio of 6% were tested. The

150 unidirectional CFRP (units weight 300g/m^2-desitiy 1.79gcm^3) had a modulus of elasticity of 230 GPa,
151 tensile strength 3900 MPa and ultimate strain 1.5%, respectively. The width of the diagonal CFRP
152 strengthening (w_f) was equal to 150mm (Fig.1) and equivalent thickness of 0.17 MPa [39]. Anchorages
153 made by rolled CFRP sheets were installed to join the CFRP sheets on both faces of the masonry wall.
154 The distance between the anchorages was 300mm. Moreover, the CFRP sheets were extended to the RC
155 frame and CFRP patches were applied at the corner zone as shown in Fig. 1.
156 The test set-up was designed to apply an axial load of 40 kN on each column and the compression force
157 of 60kN on the top beam [29]. The envelope of the cyclic test results is here presented in Fig.2 for the
158 strengthened frame with the cross braced solution. Fig.2 also shows the bare frame and the URM infill
159 frame.
160
161 **2.3 FRP strengthened masonry infills**
162 FRP strengthened infills [23–32] improve the load carrying capacity, enhancing the cyclic behavior of
163 URM infills and increasing the lateral displacement at failure. The strengthening configuration which
164 provided the best results is the one where FRPs are glued along the diagonals, which is also the preferable
165 solution in terms of cost-effectiveness.
166 FRP strengthening effectiveness develops by means of two main mechanisms. The first increases the
167 masonry compressive width strut formed along the diagonal by increasing the tensile strength of the
168 masonry in the orthogonal direction and by bridging the formed cracks. The second mechanism acts by
169 reducing the inter-story displacement demand with the FRPs acting as a tension tie (Fig. 3). In this case,
170 debonding is trigged by the panel-frame separation, where a high stress gradient is generated. The
171 debonding process starts at this corner discontinuity and proceeds to the center of the infill (Fig.3). Poor
172 performance is in general observed when the composite material is not connected or extended to the RC.

If FRPs are efficiently anchored, structural failure is triggered by CFRP mid panel debonding (or eventually rupture)

The importance of the anchorage system is also highlighted when TRM [33] or ECC [34,35] were used to strengthen the infills.

Researchers [40] showed that composite materials for this application failed at lower strain than in the uni-axial test. This can be justified by the low CFRP strength in the orthogonal direction to the fibers. The irregular masonry crack pattern, “stepped cracks”, can trigger a high strain gradient orthogonal to the fiber direction and cause FRP tensile failure. FRP with higher shear resistance in the orthogonal direction of the fibers, as for example steel reinforced polymers, are recommended for this type of application. This also highlights the advantages of using orthogonal textiles as in the TRM [33] or randomly distribute fibers as in the ECC [34,35].

The CFRP can also contribute to increasing the corner compressive resistance and additional FRP patches can increase the confinement, carry orthogonal tensile stresses and reduce the negative effect due to compression forces.

Particular attention should be given to the shear resistance of beams and columns, which may need additional strengthening due to the increase of the diagonal compression force.

3. Continuum FE model –modeling

3.1 Modelling details

The concrete frame, as well as the masonry infill, is modeled using 3D continuum elements. Only one element is used in the out of plane direction, and the symmetry plane has been used to analyze half of the structural system. The steel rebars are considered as embedded reinforcement perfectly bonded to the concrete 3D-elements and are modeled as truss elements. The CFRP material has been modeled as skin reinforcements, membrane elements perfectly bonded to the concrete and masonry surfaces. The FRP is modeled as isotropic material and not orthotropic. since the results are not significantly influenced by

this simplification. Interface elements are used to simulate the contact between masonry and RC frame. The interfaces are assumed to work only in compression and shear, the friction component for tangential sliding is assumed to be equal to 0.35.

3.2 Constitutive Material Models

The constitutive model adopted for the RC Concrete elements and the infills is the Concrete Damage-Plasticity Model (CDP) [41,42] as implemented in [43]. The parameters used to define the yield surfaces are reported in Table 1. The function adopted to describe the concrete compressive behavior is formulated by Feenstra [44] (Fig. 4a). The values used for the simulation are reported in Table 2. The infill compressive behavior, shown in Fig. 4b, is modeled using the function proposed by Lourenco [45] and the values are reported in Table 3. The tensile behavior of both concrete and infills is simulated using an exponential function (Fig. 4c). The values used are reported in Table 2 and 3 for concrete and infills, respectively. Plastic strain (ε_{pl}) is calculated as indicated in Eq.1:

$$\varepsilon = \varepsilon_{pl} + \frac{\sigma}{E} \tag{1}$$

Where σ and E are stress and Young's modulus, respectively. The values to be introduced in the strain-stress relationships are obtained from [27,29,39]. Steel reinforcement is modeled as an elastoplastic material, with hardening components. Yield stress is equal to 420 MPa, and steel ultimate strain is equal to 500 MPa. The FRP, see Fig. 5, is considered effective only in tension. In this paper, the CFRP is assumed linear elastic up to the debonding stress. Beyond this value, the loss of bond is simulated through a descending function, presented in Eq.2. This function is adapted from [46].

$$\begin{cases} \sigma = E_f \varepsilon & \varepsilon \le \varepsilon_d \\ \sigma = f_{fdd2}\left(\dfrac{\varepsilon}{\varepsilon_d}\right)^{\xi} & \varepsilon > \varepsilon_d \end{cases} \tag{2}$$

Where the debonding strain is ε_d and is equal to f_{fdd2}/E_f and ξ the softening factor assumed equal to 2.5.

The debonding stress and strain for the CFRP material are calculated by using the CNR-DT 200 [47]. Other formulations were considered, [48–51] however the Italian guidelines were preferred for their completeness. The debonding strain is calculated to be 5.6‰. This value is comparable to the experimental values obtained by [25], which shows that with a proper anchorage system large strains could be observed in the composites. Further details on the calculation of the debonding strain are provided in section 3.4, where the influence of the strengthening geometry is studied and the debonding strain is related to the stiffness of the strengthening.

3.3 Simulations results

The result obtained from the numerical simulation under monotonic loading is compared with the experimental cyclic load-displacement curve in Fig. 6. The numerical model approximates with sufficient accuracy the load-displacement envelope of the experimental results. The numerical softening part is slightly higher than the experimental envelope, because of the cyclic degradation occurred in the experiment which couldn't be captured with the numerical model. The maximum force F_{max} is calculated with high accuracy for all models. The bare frame carried a maximum force, F_{max}, of 60.7 kN (experimental values -62.2/+61.4 kN), the URM-frame, F_{max} equal to 122.3 kN (experimental values -126.0/+119.9 kN) and the strengthened frame, F_{max} of 155.3 kN (experimental values -139.9/+153.0 kN). The model captures the experimental behavior, in particular the frame infill corner separation, the formation of the diagonal compression strut, the relative orthogonal tensile action and corner crushing at masonry compressed corners, steel yielding of the longitudinal bars and shear diagonal crack in beams and columns. The FE model shows the two resisting mechanisms presented in section 2.3 and Fig.3 and illustrated in Fig. 7. High-stress localization in the CFRP is observed at the panel-concrete interface. The state of stress differences between URM and strengthened masonry infill are captured with the continuum models, it is possible to observe that the compressed region of the strengthened masonry is wider compared to URM. This evidence is herein used to define the analytical model presented in Section 4.

3.4 Parametric Study

A parametric study is carried out to study the influence of thickness and width of the FRP strips on strength and ductility of the strengthened infilled frame. t_f [0.09-0.34mm] and width w_f [100-200mm], are defined using the variable ρ_f, which is the projection of strengthening to masonry cross section surface ratio, expressed as indicated in Eq.3

$$\rho_f = A_f \cos\theta' / (h_w l_w) \quad [\%] \tag{3}$$

Where A_f and θ' are the area and the inclination of the CFRP, respectively, meanwhile h_w and l_w refer to height and length of the infill panel. The values of ρ_f, are presented in Table 4. The concept of expressing the efficiency of the reinforcement as a geometrical or mechanical percentage [50,52,53], mostly used in RC strengthening can be extended to masonry structures since it has been demonstrated that the efficiency of the reinforcement (or strengthening) is inversely proportional to its amount [53]. The intermediate debonding stress f_{fdd2} is calculated with the Italian Guidelines [47] as follows:

$$f_{fdd2} = \alpha \cdot f_{fdd} = = \alpha \sqrt{\frac{2E_t \cdot \Gamma_{Fd}}{t_f}} \tag{4}$$

Where Γ_F is calculated as indicated in [47] and $\alpha = 1.5$. The calculated f_{fdd2} and the respective stains $\varepsilon_d = f_{fdd2}/E_f$ are reported in Table 4. The calculated debonding stress are plotted versus the geometrical percentage of reinforcement in Fig. 8. Fig.8 shows that debonding strength reduces by increasing the percentage of CFRP strengthening. A small data dispersion can be observed when the f_{fdd2} is expressed as a function of ρ_f The calculated debonding strength values f_{fdd2}, as shown in Fig. 8, are fit using the following equation:

$$f_d = 120.9\rho_f^{-0.45} \quad [R^2=0.95] \tag{5}$$

The results of the numerical simulations are presented in Fig. 9. The maximum force F_{max} and the lateral force increment, ΔF due to the strengthening application are reported in Table 4. An increase of ultimate force is observed as the percentage of strengthening increases. As expected, the cracked stiffness of the structure is affected by the presence of the CFRP strips, and lower stiffness degradation for higher values of CFRP can be observed.

A higher stiffness of the cracked section corresponds to a lower displacement at F_{max}. Fig. 10 shows a linear tendency between the ρ_f and the maximum force obtained from the numerical simulation. In addition to the Load-displacement behavior of the strengthened masonry infilled frame, the continuum model explains the local behavior of the panel frame interaction. The present research is dedicated to the analytical modeling of strengthened infilled frame, and focuses on the compressive behavior of the strengthened masonry infill as the percentage of CFRP changes through the parameter ρ_f .

The previous section indicates that the width of masonry strut, i.e. compressive forces, increases due to the strengthening. This width is here calculated from the numerical model by analyzing the principal stresses and plastic strains along the diagonals. Fig.11 shows an example of how stresses and strains along the diagonals are affected by the CFRP strengthening. The values of the calculated width of the compression strut, b_w^s , are reported in Table 4. The corrective coefficient Ω_s presented in Eq (5) represents the variation of strut geometry of a strengthened panel and is calculated as the ratio between the b_w^s of the strengthened infills and the compression strut width (b_{URM}) of the URM panel:

$$\Omega_s = \frac{b_w^s}{b_{URM}} \tag{6}$$

4. Macro modelling

4.1 Macro modeling issues characteristics

Macro modeling of URM masonry infilled frame is a well-known topic. by adopting this approach a truss system is added to the bare frame to take into consideration the presence of the infill panel. Several different formulation of equivalent struts have been published in the past, these include several parameters, among which geometrical and mechanical parameters, axial forces on the columns, and presence of openings [2,3,37]. Dedicated constitutive nonlinear models have been developed [15,54–57] for nonlinear static and dynamic application. Most of the models have been developed for in-plane behavior, however out of plane behavior has also been considered [58].

Modeling the in-plane behavior of a strengthened masonry infilled frame is a recent topic. [59,60] modified the URM approach by adding a tie to represent the strengthening material. Binici and Ozcebe [60] proposed a monotonic multilinear model for the masonry strut and the FRP tie. Akin et al. [61] performed numerical simulation on RC frames with panels of different geometry, estimating the nonlinear monotonic response with reasonable accuracy. Erol et. al. [62] following the Turkish Earthquake specification [62] studied the model performance using an elastoplastic model for the masonry infills and an elastic-brittle model for the CFRP tie. Recently Koutas et al. [38] proposed a more sophisticated approach for TRM strengthened infills, in which the TRM tie, formulated as a bilinear function, is based on the concept of effective strain [50]. This model describes the strut and tie monotonic curve and provides a constitutive law for the cyclic behavior. Both models proposed by [38,61] highlight the need to modify the constitutive model for the strengthened infill, which means that strengthened infilled frame capacity cannot be computed as the sum of the URM masonry strut and tie contribution. Akin et al. [61] improved the ductility of the strengthened strut by modifying the elastic-softening law

of the URM, by adding a plastic segment before the softening phase. Koutas et al. [38], modified several parameters to characterize the strengthened infill. The model proposed by different researchers and their models' validation are strongly related to the masonry infills analyzed. Due to the complexity of the topic for URM infills, there is no univocal approach, in particular for the definition of post-cracking, hysteretic behavior, and ultimate strength. All the previously cited models can provide satisfactory results when compared to the relative experimental tests. Nevertheless, as highlighted in [38], the most difficult task is to establish the model's parameters given the complexity of the frame-infill interaction and the composite-masonry tensile interaction and its effect on the compressive forces. A correct model should provide an effective strain since it is known that the percentage of reinforcement affects the strengthening technique effectiveness [50,63]. As shown in [38,61] the effective strain does not seem to have a large impact on the final load displacement curve and further research is necessary on this issue.

4.2 Modelling details

In the present study, the frame is modeled through a distributed plasticity approach using force based fiber elements [64] with four integration points. The masonry infill strut and CFRP tie are modeled using a single equivalent strut approach and nonlinear two node link elements (Fig. 12). Shear elastic deformation is considered for the frame elements. A rigid section at the beam-column joint and a system of rigid trusses, as illustrated in Fig. 12, are used to consider the increased shear forces acting on beam and columns.

The concrete is modeled using the Chang and Mander's concrete constitutive model [65]. A compressive strength of 19.0 MPa and compressive strain of 0.25%, elastic modulus of 24.7 GPa and a tensile strength of 1.85 MPa are used in the simulations. Steel rebars are modeled using a tri-linear material with hysteretic behavior. The pinching effect is considered by using pinching factors of 0.5 and 0.37 for strain and stress, respectively.

4.2.1 URM strut

The compressive behavior of the strengthened masonry infill is calculated starting from the UR masonry model, validated using the experimental results. The model is formulated in terms of axial force (F_{axial}) and displacement (δ_{axial}). The definition of the constitutive model for the backbone curve requires the definition of the uncracked state up to the cracking shear force V_{cr} (a), the cracked state up to it maximum resistance V_u (b), the softening part (c), and the residual strength V_r. The first two segments of the curve are replaced by a parabolic function as shown in Fig. 13 and Eq.6. The advantages of using a parabolic curve lie in the definition of only two variables V_u and K_m, where K_m is the secant stiffness to ultimate resistance V_u calculated from the elastic properties of the masonry infill. The function that describes the parabolic behavior follows:

$$V = V_u\left[\frac{2\delta}{V_u}K_m - \left(\frac{\delta}{V_u}K_m\right)^2\right] \qquad 0 \le \delta \le \delta_u \tag{7}$$

Where $\delta_u = V_u/K_m$ represents the displacement at V_u. For the model presented in this paper, the tangential elastic stiffness K, is equal to $2K_m$. The softening behavior is defined as a linear function up to a residual shear resistance V_r and is governed by the parameter beta β as follows in Eq. 8:

$$V = V_u - \beta K_m\left(\delta - \delta_u\right) \qquad \delta_u < \delta \le \delta_r \tag{8}$$

$$V = V_r \qquad \delta > \delta_r$$

The parameter β is assumed equal to 0.25 and the residual strength V_r has been set equal to 0.05 V_u. Satisfactory results are obtained also using a trilinear backbone curve (Fig.13) for which the cracking force and displacement are adopted as $V_{cr} = 0.5 \cdot V_u$ and $\delta_{cr} = V_u/4K_m$, respectively as shown in Fig. 17.

The secant horizontal stiffness K_m is calculated as indicated in Eq. 8 [38,56], assuming the masonry strut of thickness t_w, length d_w, theoretical width b_w and elastic modulus E_w:

$$K_m = \frac{E_w t_w b_w}{d_w} \cos^2 \theta \tag{9}$$

where θ is the inclination of the masonry strut. The geometry of the equivalent strut is in general related to the geometrical and mechanical properties of the sub-systems: frame and infill, by means of the λ parameter originally proposed by [66] The relative stiffness and the relative strength between infill panels and columns govern the overall behavior and system failure sequence, λ is defined following the Stafford Smith approach [66] as a function of the relative infill-to frame stiffness as:

$$\lambda = \left(\frac{E_w t_w \sin 2\theta}{4 E_c I_c h_w} \right)^{1/4} \tag{10}$$

where E_w and E_c are the elastic modulus of the masonry strut and concrete, I_c is the moment of inertia of the column and h_w is the height of the infill panel. The strut width is calculated using the formulation proposed by Mainstone [67] and adopted in FEMA-247[68] and FEMA-306[4], b_w is calculated using the empirically derived equation presented in Eq.(11)

$$b_w = 0.175 \cdot d_w \cdot (\lambda H)^{-0.4} \tag{11}$$

The orthotropic elastic modulus of the masonry under compression along the diagonal direction, E_w is calculated using Eq. 13. [69]:

$$E_w = \frac{1}{\frac{1}{E_0}\cos^4\theta + \left(-\frac{2 \cdot \nu}{E_0} + \frac{1}{G}\right)\cos^2\theta \sin^2\theta + \frac{1}{E_{90}}\sin^4\theta} \tag{12}$$

where E_0 and E_{90} are Young's modulus along the direction parallel to the holes and perpendicular to the holes, respectively. The ultimate strength of the infill depends on the masonry infills properties and the failure mechanism. The ultimate strength of the infill is defined following the formulation proposed by Mainstone [70]:

$$V_u = 0.56(\lambda H)^{-0.875} f_w H t_w \cos^2 \theta \tag{13}$$

where H is the story height, and f_w is the compressive masonry strength, which is assumed as 4.85 MPa as shown

366 in Table 5. The geometric transformation from $V-\delta$, shear – inter-story drift behavior to $F_{axial}-\delta_{axial}$ axial
367 force-axial displacement is shown in Eq.s 15-17:

$$V_{V-d} = F_{axial}\cos\theta \tag{14}$$

368

$$K_{axial} = K_{V-d} / \cos^2\theta \tag{15}$$

369

$$dL_{str} = \left(\frac{L}{H}\sin\theta\right)\delta \tag{16}$$

370 where dL_{str} is the axial shortening of the masonry strut.
371 The cycle infill behavior for both strengthened and URM strut was modeled with degraded linear
372 unloading/reloading stiffness according to the Karsan-Jirsa model [71]. In the case of a hysteretic
373 behavior, a pinching factor of 0.42 and 0.37 is applied to the axial displacement and force, respectively.
374 Each compression strut is assumed to be effective only in compression.

375
376 **4.2.2 Strengthened masonry strut**
377
378 In analogy to the models proposed for infilled frames with openings [72,73], where the openings are
379 considered by means of a reduction factor affecting stiffness and strength of the masonry infill, the
380 proposed model considers the presence of the strengthening with a corrective coefficient which increases
381 the stiffness and strength of the strengthened infilled frame. The calculated masonry strut width presented
382 in Table 4, is modified with a calibrated coefficient factor to increase the masonry strut width proposed
383 by [67]. In order to calculate the coefficient, Ω_s, ρ_s are plotted vs the b_w^s normalized by the length b_w.
384 Fig. 14 shows the coefficients, Ω_s for different percentages of CFRP strengthening. Eq. 18 is the fitting
385 function that provides the value of Ω_s:

$$\Omega_s = 0.24\ln\rho_f + 2.27 \qquad R^2=0.86 \tag{18}$$

The strut width b_w used for URM is modified with the value $\Omega_s \cdot b_w$ to account for the strengthening effect. Therefore, the secant stiffness K_m is multiplied by the coefficient Ω_s.

$$K_s = \Omega_s K_m = \Omega_s \frac{E_w t_w b_w}{d_w} \cos^2 \theta \tag{19}$$

Table 5 and Fig. 13 show the comparison between the strengthened and URM panel models.

4.2.3 Tensile behavior of the retrofitted infill

The tensile behavior of the CFRP tie is modeled modifying the models presented in literature [38,61]. The model is based on a bilinear function as shown in Fig. 15. The first branch represents the elastic part and the second the softening part, forces in the FRP are derived using Eq. 20 and 21:

$$F_{FRP} = K_{FRP} \cdot \delta_{axial} \qquad 0 < \delta_{axial} \leq \delta_{\max} \tag{20}$$

$$F_{FRP} = F_{FRP}^{\max} - \gamma K_{FRP} \cdot \left(\delta_{axial} - \delta_{\max}\right) \qquad \delta_{axial} > \delta_{\max} \tag{21}$$

The model requires the definition of the elastic stiffness K_{FRP}, the FRP maximum strength $F_{FRP}^{\max}$, and the parameter γ, used in this paper to calculate the slope of the softening branch. The elastic stiffness is calculated as presented in Eq.(22):

$$K_{FRP} = \frac{E_f A_f}{L_{eff}} \tag{22}$$

where E_f and A_f are the elastic modulus and area of the FRP, respectively. L_{eff}, is the effective length as shown in Koutas [38]. L_{eff} is used to calculate the tensile tie stiffness and it is defined considering the masonry cracks along the diagonal. The L_{eff} is a reduced length of the infill diagonal (i.e. the length of the FRP tie) and is assumed as 0.5 d_w. The maximums strength of the FRP tie, $F_{FRP}^{\max}$, is the product

between $K_{FRP} \cdot \delta_{\max}$ or rather: $K_{FRP} \cdot \varepsilon'_d \cdot d_w$ where the ε'_d is a smeared average strain in the CFRP tie. Both values of L_{eff} and ε'_d are not easily calculable, for this reason, the FRP tie model is calibrated in terms of maximum strength $F_{FRP}^{\max}$, which is a function of both L_{eff} and ε'_d. The value used for $F_{FRP}^{\max}$ is 46.9 kN for the experimental cross brace configuration with CFRP width and thickness, 150mm and 0.17mm, respectively. The calibrated value is calculated by considering the increment of lateral maximum load provided by the presence of CFRP strengthening during the experimental tests. The value of $F_{FRP}^{\max}$, for the discussed strengthening configuration, correspond to L_{eff} of 0.5 d_w and ε'_d equal to 2.00‰, which is a value smaller than the one used in the continuum modeling. In the continuum model the local strain is considered, instead an average strain along the entire length of the CFRP tie is assumed in the macro model. Similar strain values are used also by [61,62]. Cyclic behavior of the FRP tie- tension model is characterized by an hysteretic behavior with pinching factors of 0.7 and 0.1 for strain and stress, respectively. The constitutive model of the CFRP is assumed to work only in tension.

5 Numerical Simulations

5.1 Procedure validation

Figs. 16-18 show the comparison between the experimental cyclic tests and the macro model results. By observing Fig. 16 and Fig 17 it is possible to notice how the calculated Force-Displacement curves reproduce the experimental results with good accuracy in terms of force-displacement relationship and energy dissipation. Fig. 17 indicates that the proposed parabolic-linear model simulates well the stiffness, strength and degradation of the masonry infilled frame. The trilinear backbone curve with hysteretic cyclic behavior is also shown in Fig. 17. Also this model, with the simplified assumptions of V_{cr} and δ_{cr}, presented in the previous chapter., predicts well the behavior. In terms of maximum lateral force, the bare frame carried a maximum force, F_{max}, of 62.6 kN (experimental values -62.2/+61.4 kN), the URM-frame a F_{max} equal to 121.2 kN (experimental values -126.0/+119.9 kN). Fig. 18 shows the comparison among

the experimental cyclic envelope, the continuum model and the macro model. The macro and the continuum model describe with good accuracy the experimental results. The cyclic behavior and the maximum lateral force are correctly estimated F_{max} equal to 155.4 kN (experimental values -139.9/+153.0 kN).

These simulations were important for the calibration of the RC frame and URM panel, in order to validate the proposed model for strengthened masonry panel and CFRP tie.

5.1 Influence of the tensile tie model

A relevant aspect of the discussed approach lies in the constitutive model parameters used to derive the FRP tie behavior. Therefore, the influence of the parameters $\varepsilon_d^{'}$, L_{eff}, γ, on the infilled frame response are analyzed. Fig. 19a shows the influence of the average smeared strain. Three different values are investigated $\varepsilon_d^{'}$=1.0, 2.0, 3.0 ‰, the values of L_{eff} and γ are fixed. Fig. 19a indicates that for a fixed value of the initial branch stiffness, the strain value significantly affects the maximum lateral force of the structural system, because in the proposed model the average strain is used to calculate the $F_{\max}^{FRP}$. Fig. 19.b shows the influence of the effective length on the stiffness of the structural system. Three different values are investigated L_{eff} =0.25,0.50,1.00, $\varepsilon_d^{'}$ and γ are fixed.

The effect of L_{eff} on the stiffness andmaximum lateral load is small for values of L_{eff} ranging between $0.25\,d_{\inf}$ and $0.5\,d_{\inf}$. Fig. 19.c shows the influence of the softening parameters γ. Three different values are investigated γ= 1e-4, 0.05,0.5, $\varepsilon_d^{'}$ and L_{eff} are fixed. These results show that γ should be assumed between 1e-4, and 0.05 as also shown in [38].

The parametric analyses show that the parameters $F_{\max}^{FRP}$ and $\varepsilon_d^{'}$. influence greatly the numerical response, while L_{eff} and γ can be set equal to $0.50\,d_{\inf}$ and 0.05,. respectively-

5.2 Compression -Tension constitutive model validation

In this section, the proposed macro model is validated with the continuum model presented in Chapter 3. Different geometries and thicknesses of CFRP strengthening are considered in this study. The initial stiffness of the strut is calculated using the coefficient Ω_s in Table 4 and $F_{\max}^{FRP}$ is calculated for the different percentage of CFRP. The smeared average strain $\varepsilon_d^{'}$ to obtain $F_{\max}^{FRP}$, is calculated using the CNR-DT200 model [47]. The values of $F_{\max}^{FRP}$, $\delta_{\max}$, $\varepsilon_d^{'}$ and K_{FRP} are indicated in Table 6.

Eq. 23 is the fitting curve of $\varepsilon_d^{'}$ for different values of ρ_f.

$$\varepsilon_d^{'} = 0.186 \cdot \rho_f^{-0.45} \; [R^2=0.95] \tag{23}$$

Eq. 23 is Eq. 5 written in terms of strain instead of stress and scaled in order to represent the average smeared debonding strain for the tensile FRP tie instead of the local debonding strain. $\varepsilon_d^{'}$ ranges between 1.3 and 3.1 ‰, however, for practical and design purposes $\varepsilon_d^{'}$ can be limited to a range of 1.5-2.0‰.

All the results of the performed numerical simulation are presented in Table 5. Fig. 20 shows the load displacement curve of three strengthening configurations with different CFRP thickness and width. The macro model provides very similar results to the more sophisticated continuum model. The proposed macro model provides satisfactory results to predict the seismic behavior of FRP strengthened infill panels.

6. Conclusion

The present work investigates the structural behavior of CFRP strengthened infilled frame. The main purpose of this study is to propose an analytical formulation for masonry panel strengthened with different percentages of CFRP. The analytical model is based on the definition of cyclic constitutive models for the masonry strut acting in compression and for the CFRP tie acting in tension.

A continuum FE model, validated using experimental results is used to develop a parametric study to study the influence of the CFRP thickness and width on the lateral force- displacement behavior. The analyses show that the compression masonry strut width and the debonding stress are influenced by the strengthening percentage. In particular, the compression strut width increases by increasing the strengthening percentage and the debonding stress decreases by increasing the strengthening thickness. The analytical formulation uses a parabolic-linear function constitutive law to model the masonry compression strut. The URM strut width is modified to consider the effect of strengthening using a corrective coefficient calibrated numerically. Bilinear function constitutive law is used for the CFRP tie. The model parameters are calibrated with parametric analyses which indicated that the FRP strength is the parameter affecting the most the results. The model proposed predicts with good accuracy the cyclic behavior of CFRP strengthened masonry infilled frame. It is computationally efficient and can be used to model the strengthened infills of existing RC frame structures. The model can be easily extended to other type of strengthening solutions and materials.

Acknowledgements

The authors wish to acknowledge the support provided by the ReLUIS funded by the Italian Department of Civil Protection Project: 00000-0000).

References

[1] Murty CVR, Brzev S, Faison H, Comartin CD, Irfanoglu A. AT RISK: The Seismic Performance of Reinforced Concrete Frame Buildings with Masonry Infill Walls-Publication Number WHE-2006-03 2006:82.

[2] Asteris PG, Antoniou ST, Sophianopoulos DS, Chrysostomou CZ. Mathematical Macromodeling of Infilled Frames: State of the Art. J Struct Eng 2011;137:1508–17.

[3] Tarque N, Candido L, Camata G, Spacone E. Masonry infilled frame structures: state-of-the-art review of numerical modelling. Earthquakes Struct 2015;8:225–51.

[4] Applied Technology Council (ATC-43 Project). FEMA-306, Evaluation of earthquake damaged concrete and masonry wall buildings-Basic Procedures Manual. Federal Emergency Management Agency, FEMA-306, Washinton D.C.; 1999.

[5] European Committee for Standardization. Eurocode 8: Design of structures for earthquake

resistance - Part 1: General Rules, Seismic Actions and Rules for Buildings, prEN 1998-1. Brussel,Belgium: 1998.
[6] Fardis MN, Bousias SN, Franchioni G, Panagiotakos TB. Seismic response and design of RC structures with plan-eccentric masonry infills. Earthq Eng Struct Dyn 1999;28:173–91.
[7] Liberatore L, Decanini LD. Effects of infills on the seismic response of high-rise RC buildings designed as bare according to Eurocode 8. Ing Sismica 2011;28:7–23.
[8] Sezen H, Whittaker AS, Elwood KJ, Mosalam KM. Performance of reinforced concrete buildings during the August 17, 1999 Kocaeli, Turkey earthquake, and seismic design and construction practise in Turkey. Eng Struct 2003;25:103–14.
[9] Aschheim M. Kocaeli, Turkey, Earthquake reconnaissance report,Supplement A to Volume 16. Earthquake Spectra. 2000;December:237–279.
[10] Hugo B. Seismic Conceptual Design of Buildings – Basic principles for engineers, architects, building owners, and authorities 203AD:81.
[11] Kaushik HB, Rai DC, Jain SK. Code Approaches to Seismic Design of Masonry-Infilled Reinforced Concrete Frames: A State-of-the-Art Review. Earthq Spectra 2006;22:961–83.
[12] Dolšek M, Faijfar P. Soft Storey effects in Uniformly Infilled Reinforced Concrete Frames. J Earthq Eng 2001;5:1–12.
[13] Akin LA. Behaviour of Reinforced Concrete Frames with Masorny Infills in Seismic Regions. Purdue University West Lafayette, Indiana, 2006.
[14] Hassan AF, Sozen MA. Seismic Vulnerability Assessment of Low-Rise Buildings in Regions with Infrequent Earthquakes. ACI Struct J 1997;94:31–9.
[15] Fardis MN, Panagiotakos TB. Seismic design and response of bare and masonry infilled reinforced concrete buildings. Part I: Bare Structures. J Earthq Eng 1997;1:219–56.
[16] Mehrabi AB, Shing PB, Schuller MP, Noland JL. Experimental Evaluation of Masonry-Infilled RC Frames. J Struct Eng 1996;122:228–37.
[17] Pujol S, Fick D. The test of a full-scale three-story RC structure with masonry infill walls. Eng Struct 2010;32:3112–21.
[18] Kakaletsis DJ, Karayannis CG. Influence of masonry strength and openings on infilled RC frames under cyclic loading. J Earthq Eng 2008;12:197–221.
[19] Decanini LD, Mollaioli F, Mura F, Saragoni R. Seismic performance of masonry infilled RC frames. Proc. 13th World Conf. Earthq. Eng. 13th WCEE, Vancouver, Canada.: 2004.
[20] Ozkaynak H, Yuksel E, Yalcin C, Dindar AA, Buyukozturk O. Masonry infill walls in reinforced concrete frames as a source of structural damping. Earthq Eng Struct Dyn 2014;43:949–68.
[21] Comité euro-international du béton. RC frames under earthquake loading : state of the art report. T. Telford; 1996.
[22] ltın, S & Anil, Özgür & Kopraman, Y & Belgin, Ç. Strengthening masonry infill walls with reinforced plaster. ICE Proceedings Structures and Buildings. 2010. 163. 10.1680/stbu.2010.163.5.331.
[23] Naguib WI, Talaat M, Citipitioglu A. FRP Retrofit for Collapse Mitigation of RC Frames with URM Infills: 3-D Computational Modeling of an As-Built and Retrofitted One Story Building. Improv. Seism. Perform. Exist. Build. Other Struct., 2009, p. 1086–1092.
[24] Akin E, Canbay E, Binici B, Ozcebe G. Testing and analysis of infilled reinforced concrete frames strengthened with CFRP reinforcement. J Reinf Plast Compos 2011;30:1605–20.
[25] Altin S, Anil Ö, Kara ME, Kaya M. An experimental study on strengthening of masonry infilled RC frames using diagonal CFRP strips. Compos Part B Eng 2008;39:680–93.
[26] Altin S, Anil Ö, Kopraman Y, Kara ME. Hysteretic behavior of RC shear walls strengthened with CFRP strips. Compos Part B Eng 2013;44:321–9.

[27] Yuksel E, Ozkaynak H, Buyukozturk O, Yalcin C, Dindar AA, Surmeli M, et al. Performance of alternative CFRP retrofitting schemes used in infilled RC frames. Constr Build Mater 2010;24:596–609.
[28] Erol G, Karadogan HF. Seismic strengthening of infilled reinforced concrete frames by CFRP. Compos Part B Eng 2016;91:473–91.
[29] Ozkaynak H, Yuksel E, Buyukozturk O, Yalcin C, Dindar AA. Quasi-static and pseudo-dynamic testing of infilled RC frames retrofitted with CFRP material. Compos Part B Eng 2011;42:238–63.
[30] Tumialan, J. G., San Bartolome A., Li T. and Nanni A.. Behavior of Urm Infill Walls Strengthened with Frp Bars. 2003. Advancing with Composites - Plast-2003, proc. of the Int. Conf., Milan, Italy.
[31] Saatcioglu M, Serrato F, Foo S. Seismic Performance of Masonry Infill Walls Retrofitted With CFRP Sheets. ACI— SP230 7th Int. Symp. Fiber-Reinforced Polym. Reinf. Concr. Struct., 2005, p. 341–354.
[32] Yuksel E, Ilki A, Erol G, Demir C, Karadogan HF. Seismic retrofit of infilled Reinforce Concrete Frames with CFRP Composites. Adv. Earthq. Eng. Urban Risk Reduct. - NATO Sci. Ser. IV. Earth Environ. Sci. – Vol. 66, 2005, p. 562.
[33] Koutas L, Bousias SN, Triantafillou TC. Seismic Strengthening of Masonry-Infilled RC Frames with TRM: Experimental Study. J Compos Constr 2015;19:4014048.
[34] Koutromanos I, Kyriakides M, Stavridis A, Billington S, Shing PB. Shake-Table Tests of a 3-Story Masonry-Infilled RC Frame Retrofitted with Composite Materials. J Struct Eng 2013;139:1340–51.
[35] Kyriakides MA, Billington SL. Cyclic Response of Nonductile Reinforced Concrete Frames with Unreinforced Masonry Infills Retrofitted with Engineered Cementitious Composites. J Struct Eng 2014;140:4013046.
[36] Asteris PG, Cotsovos DM, Chrysostomou CZ, Mohebkhah A, Al-Chaar GK. Mathematical micromodeling of infilled frames: State of the art. Eng Struct 2013;56:1905–21.
[37] Di Trapani F, Macaluso G, Cavaleri L, Papia M. Masonry infills and RC frames interaction: literature overview and state of the art of macromodeling approach. Eur J Environ Civ Eng 2015;19:1059–95.
[38] Koutas L, Triantafillou TC, Bousias SN. Analytical Modeling of Masonry-Infilled RC Frames Retrofitted with Textile-Reinforced Mortar. J Compos Constr 2015;19:4014082.
[39] Ozsayin B, Yilmaz E, Ispir M, Ozkaynak H, Yuksel E, Ilki A. Characteristics of CFRP retrofitted hollow brick infill walls of reinforced concrete frames. Constr Build Mater 2011;25:4017–24.
[40] Daniel M, Ishai O. Engineering Mechanics of Composite Materials. 2005.
[41] Lee J, Fenves GL. A plastic-damage concrete model for earthquake analysis of dams. Earthq Eng Struct Dyn 1998;27:937–56.
[42] Lubliner J, Oliver J, Oller S, Oñate E. A plastic-damage model for concrete. Int J Solids Struct 1989;25:299–326.
[43] SIMULIA. “Abaqus Theory Manual”, Version 6.12, Dassault Systémes Simulia Corp., Providence, RI, 2012b n.d.
[44] Feenstra PH. Computational aspects of biaxial stress in plain and reinforced concrete. Ph.D. thesis, Delft University of Technology., 1993.
[45] Lourenço PB. Computational strategies for masonry structures. PhD Thesis, Delft University of Technology, Deft, The Netherlands., 1996.
[46] Rizzo A, De Lorenzis L. Modeling of debonding failure for RC beams strengthened in shear with NSM FRP reinforcement. Constr Build Mater 2009;23:1568–77.
[47] CNR. National Research Council. Guide for design and construction of externally bonded FRP

systems for strengthening existing structures. 2012. CNR-DT200 2012.
[48] ACI Committee 440. 440.7R-10 Guide for Design & Constr of Externally Bonded FRP Systems for Strengthening Unreinforced Masonry Structures 2010:46.
[49] Tomazevic M, Lutman M, Pertrovic L. In plane behavior of reinforced masonrywalls subjected to cyclic lateral loads. Report to the ministry of science andtechnology of republic of Slovenia, parts 1 and 2. Ljubljana, Slovenia;1993
[50] Triantafillou T., Antonopoulos CP. Design of concrete flexural members strengthened in shear with FRP. J Compos Constr 2000;4:198–205.
[51] AC125. Acceptance criteria for concrete and reinforced or unreinforced masonry strengthened using fiber reinforced polymers (FRP) composite systems. Int. Conf. Build. Off., 2001.
[52] Breveglieri M, Aprile A, Barros JAO. Embedded Through-Section shear strengthening technique using steel and CFRP bars in RC beams of different percentage of existing stirrups. Compos Struct 2015;126:101–13.
[53] Tomazevic M. Masonry structures in seismic areas a state of the art report. Proc., 9th Eur. Conf. Earthq. Eng. Moscow., 1990.
[54] Klingler R, Bertero V. Earthquake resistance of infilled frames. J Struct Div ASCE 1978;104:973–989.
[55] Crisafulli FJ, Carr AJ. Proposed Macro-model for the analysis of infilled frame structures. Bull New Zeal Soc Earthq Eng 2007;40:69–77.
[56] Bertoldi SH, Decanini LD, Gavarini C. Telai tamponati soggetti ad azioni sismiche, un modello semplificat: confronto sperimentale e numerico. Atti del 6 Convegno Naz. ANIDIS, vol.2, Perugia, 13-15 Ottobre 1993 [in Ital., 1993, p. 329–40.
[57] Furtado A, Rodrigues H, Arêde A, Varum H. Simplified macro-model for infill masonry walls considering the out-of-plane behaviour. Earthq Eng Struct Dyn 2016;45:507–24.
[58] Kadysiewski S, Mosalam KM. Modeling of Unreinforced Masonry Infill Walls Considering In-Plane and Out-of-Plane Interaction. 2009. PEER Report 2008/102 Pacific Earthquake Engineering Research Center College of Engineering University of California, Berkeley, January.
[59] Fédération internationale du béton. Retrofitting of concrete structures by externally bonded FRPs : with emphasis on seismic applications. International Federation for Structural Concrete; 2006.
[60] Binici B, Ozcebe G. Analysis of infilled reinforced concrete frames strengthened with FRPs. Adv. Earthq. Eng. urban risk reduction, S. T. Wasti G. Ozcebe, eds., Vol. 66, NATO Sci. Ser. Earth Environ. Sci. Springer, Amsterdam, Netherlands, 2006, p. 455–471.
[61] Akın E, Özcebe G, Canbay E, Binici B. Numerical Study on CFRP Strengthening of Reinforced Concrete Frames with Masonry Infill Walls. J Compos Constr 2014;18:4013034.
[62] Ministry of Public Works and Settlement. Turkish earthquake code: specifications for buildings to be built in earthquake zones, Ankara, Turkey 2007.
[63] Breveglieri M, Aprile A, Barros JAO. RC beams strengthened in shear using the Embedded Through-Section technique: experimental results and analytical formulation. Compos Part B Eng 2016;89:266–81.
[64] McKenna F, Fenves GL, Scott MH, Jeremic B. Open system for earthquake engineering simulation (OpenSees). 2000. University of California, Berkeley, CA
[65] Chang GA, Mander JB. Seismic Energy Based Fatigue Damage Analysis of Bridge Columns. 1994.
[66] Stafford Smith B. Methods for predicting the lateral stiffness and strength of multi-storey infilled frames. Build Sci 1967;2:247–57.
[67] Mainstone RJ. Supplementary note on the stiffness and strength of infilled frames. Build Res

Station CP 13/74, Build Res Establ UK 1974.
[68] Emergency MAF. NEHRP commentary of the guidelines for seismic rehabilittion of buildings. FEMA-274. 1997.
[69] El-Dakhakhni WW, Elgaaly M, Hamid AA. Three-Strut Model for Concrete Masonry-Infilled Steel Frames. J Struct Eng 2003;129:177–85.
[70] Mainstone RJ. On the stiffness and strengths of infilled frames. Proc Inst Civ Eng 1971;Supplement:57–90.
[71] Karsan I, Jirsa J. Behavior of Concrete Under Compressive Loadings. J Struct Div 1969;95:2543–64.
[72] Decanini LD, Liberatore L, Mollaioli F. Strength and stiffness reduction factors for infilled frames with openings. Earthq Eng Eng Vib 2014;13:437–54.
[73] Mohammadi M, Nikfar F. Strength and Stiffness of Masonry-Infilled Frames with Central Openings Based on Experimental Results. J Struct Eng 2013;139:974–84.

Table 1 Parameters used for the Concrete – Damage Plasticity model [ref]

Concrete Damage Plasticity Parameters	
Concrete dilatancy angle	30°
Masonry dilatancy angle	35°
Eccentricity	0.01
f_{b0}/f_{c0}	1.16
K	1
Viscosity Parameter	0.0001

659 **Table 2** Concrete material parameters

Compressive behavior [a]	
Poisson's ratio (ν)	0.15
Initial Young's modulus (E)	25.9 MPa
Compressive strength (f_c)	19.0 MPa
Compressive strain at peak ($\varepsilon_{p)}$	0.0025 [-]
Compressive fracture energy (G_c)	10.0 N/mm
Tensile behavior: Exponential model	
Tensile strength (f_{tm})	1.8 MPa
Fracture Energy in tension (G_f)	0.065 N/mm

660

661 **Table 3** Infill material parameters

Compressive behavior	
Poisson's ratio (ν)	0.35
Initial Young's modulus (E)	4.99 MPa
Compressive strength (f_c)	4.15 Mpa
Compressive strain at peak ($\varepsilon_{p)}$	0.0048 [-]
Compressive fracture energy (G_c)	1 N/mm
Tensile behavior: Exponential model	
Tensile strength (f_{tm})	= 0.92 MPa,
Fracture Energy in tension (G_f)	= 0.01 N/mm

662

663

664 **Table 4** Percentage of CFRP strengthening ρ_f [‰] as for different width [t_f] and thickness [w_f]

w_f	t_f	ρ_f	f_{dd2}	ε_d	F_{max}	ΔF	b_w^s	Ω_s
[mm]	**[mm]**	**[%]**	**[MPa]**	**[--]**	**[kN]**	**[kN]**	**[m]**	**[--]**
100	0.09	0.0017	2.00E+03	8.71E-03	136.9	14.0	0.49	1.17
	0.17	0.0035	1.42E+03	6.16E-03	143.1	20.2	0.56	1.32
	0.26	0.0052	1.16E+03	5.03E-03	148.8	25.9	0.63	1.41
	0.34	0.0069	1.00E+03	4.35E-03	152.4	29.5	0.62	1.48
150	0.09	0.0026	1.83E+03	7.98E-03	145.3	22.4	0.49	1.25
	0.17	0.0052	1.30E+03	5.64E-03	153.6	30.7	0.56	1.41
	0.26	0.0078	1.06E+03	4.61E-03	161.1	38.2	0.65	1.51
	0.34	0.0104	9.17E+02	3.99E-03	168.8	45.9	0.62	1.58
200	0.09	0.0035	1.66E+03	7.23E-03	150.9	28.0	0.58	1.32
	0.17	0.0069	1.18E+03	5.11E-03	160.0	37.1	0.61	1.48
	0.26	0.0104	9.60E+02	4.18E-03	169.2	46.3	0.67	1.58
	0.34	0.0138	8.32E+02	3.62E-03	174.5	51.6	0.70	1.65

665

666

667 **Table 5** Properties of the strut used in the analysis

Variable	URM	Strengthened panel
λH [m]	2.09	
b_w [m]	0.160	0.142 Ω_s (0.227)
E_W [MPa]	2.09	
t_w [m]	0.07	
d_w [m]	1.23	
K_m [MPa]	12.1	17.3
f_w [MPa]	4.85	4.85
V_u [kN]	75.1	75.1

668

669

Table 6 Properties of the FRP tie and results

w_f	t_f	ρ_f	δ_{max}	$\varepsilon_d^{'}$	K_{FRP}	F_{max}^{FRP}	F_{max}	Δ
[mm]	**[mm]**	**[%]**	**[mm]**	**[‰]**	**[MPa]**	**[KN]**	**[KN]**	[%]
100	0.09	0.0017	3.78	3.1	6.74E+06	25.48	143.6	4.9
	0.17	0.0035	2.68	2.2	1.27E+07	34.17	148.9	4.1
	0.26	0.0052	2.19	1.8	1.95E+07	42.69	154.5	3.8
	0.34	0.0069	1.84	1.5	2.62E+07	48.12	157.8	3.5
150	0.09	0.0026	3.46	2.8	1.01E+07	34.97	150.4	3.5
	0.17	0.0052	2.46	2.0	1.91E+07	46.92	155.4	1.2
	0.26	0.0078	2.00	1.6	2.92E+07	58.51	166.2	3.2
	0.34	0.0104	1.73	1.4	3.82E+07	66.19	171.3	1.5
200	0.09	0.0035	3.14	2.6	1.35E+07	42.29	155.8	3.2
	0.17	0.0069	2.23	1.8	2.55E+07	56.79	165.4	3.4
	0.26	0.0104	1.82	1.5	3.89E+07	70.66	175.1	3.5
	0.34	0.0138	1.57	1.3	5.09E+07	80.08	181.4	4.0

Figure captions

Fig.1 Experimental frame tested by Yuksel et al. [27].

Fig. 2 Force-displacement envelop of the experimental results [27].

Fig.3 FRP resisting mechanism.

Fig.4 Stress-Strain constitutive models for (a) Concrete in compression, (b) Masonry in Compression, (c) Exponential traction model for both concrete and masonry.

Fig.5 Stress-Strain constitutive models for CFRP.

Fig.6 Force – displacement comparison between experimental and continuum model results.

Fig. 7 (a) Plastic Strain Min.Principal (only the masonry infill has been displayed) (b) Stress Max.Principal before F_{max} (only the CFRP on the masonry has been displayed)

Fig.8 Estimated debonding strain using the CNR-DT 200 [47] plotted versus the geometrical percentage of reinforcement.

Fig 9 Parametric study- numerical force displacemet relationship for diffrerent CFRP thickness [0.09-0.34 mm] and width: (a) 100mm, (b) 150mm, (c) 200mm.

Fig. 10 Parametric study – Maximum attained load vs the percentage of CFRP strengthening.

Fig. 11 Plastic strain comparison between strengthened and un-strengthened infill panel.

Fig. 12 Macro model of the strengthened masonry infilled frame.

Fig.13 Strut model

Fig 14 Ω_s coefficient the are plotted vs the ρ_s

Fig 15 CFRP Tensile Tie model

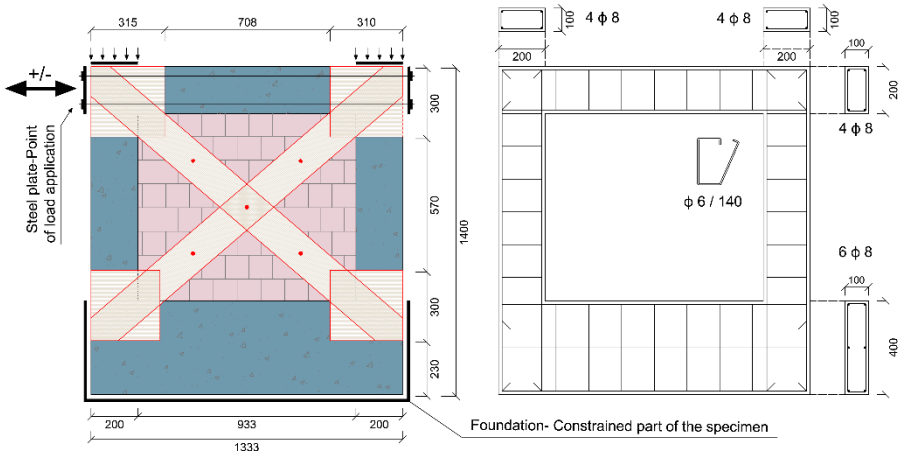

699

700 Fig.1 Experimental frame tested by Yuksel et al. [27]

701

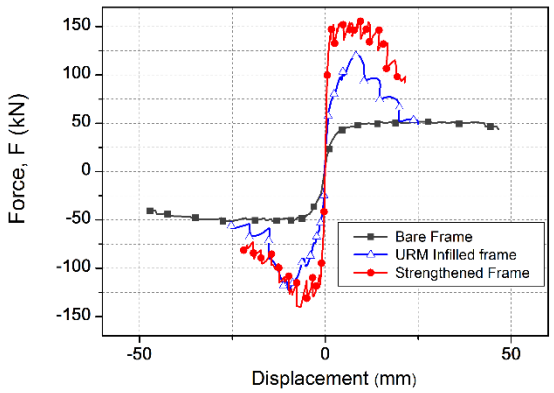

Fig. 2 Force-displacement envelope of the experimental results [27]

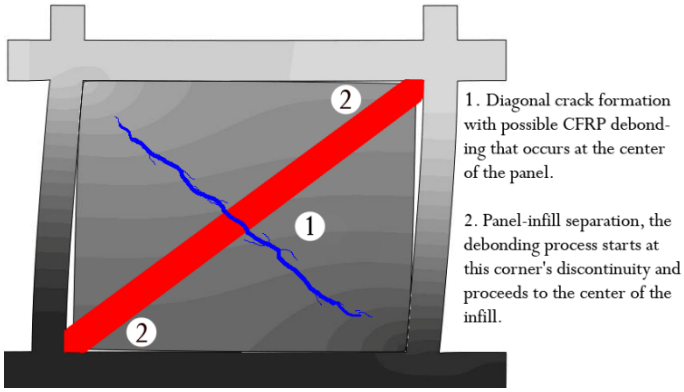

705

706 Fig. 3 FRP resisting mechanism

707

708

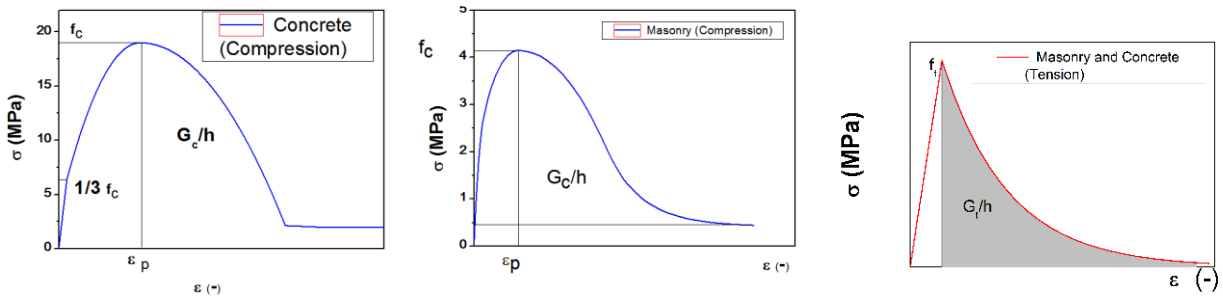

(a) (b) (c)

Fig. 4 Stress Strain constitutive models for (a) Concrete in compression, (b) Masonry in Compression, (c) Exponential traction model for both concrete and masonry.

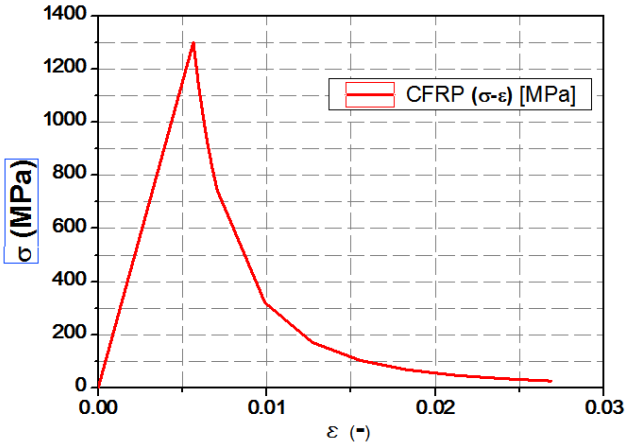

714 Fig. 5 Stress Strain constitutive models for CFRP

715

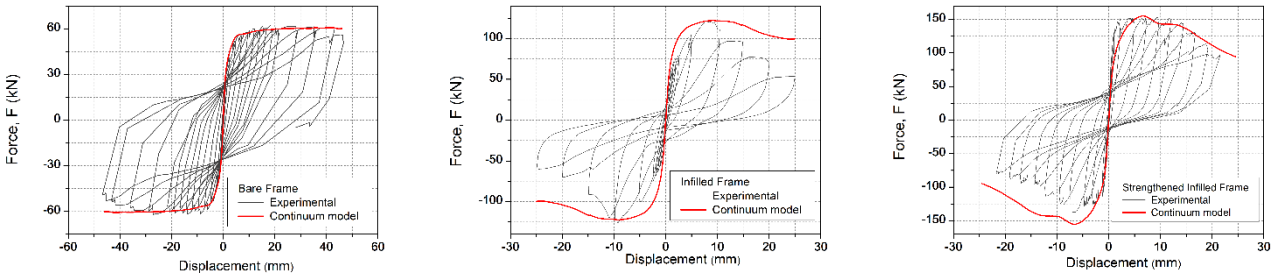

Bare Frame URM infilled Frame R-URM infilled Frame

716
717 Fig. 6 Force – displacement comparison between experimental and continuum model results.
718

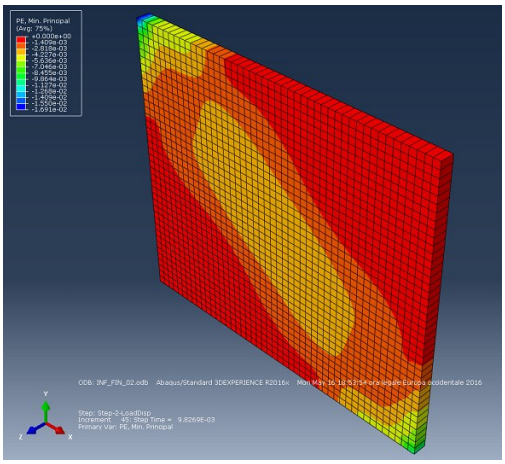

(a)

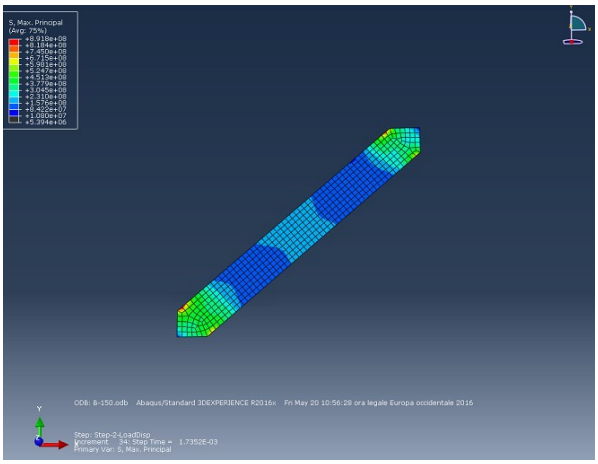

(b)

719

720 Fig. 7 (a) Plastic Strain Min.Principal (only the masonry infill is displayed) (b) Stress Max.Principal before F_{max} (only the
721 CFRP on the masonry is displayed)

722

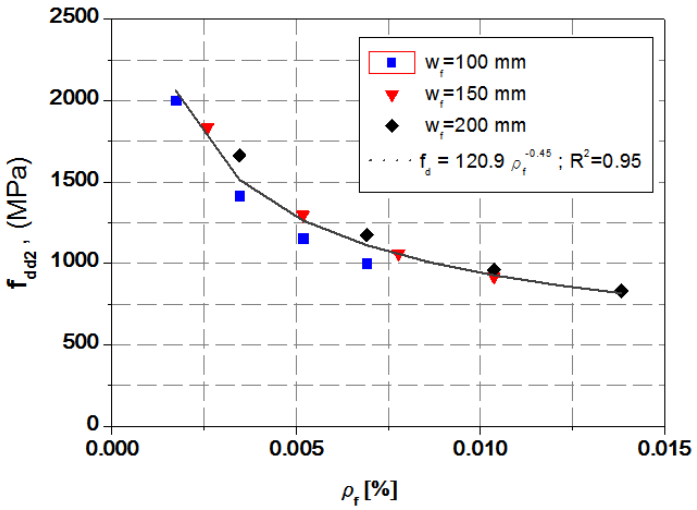

723

724 Fig. 8 Estimated debonding strength using CNR-DT 200 [47] plotted versus the geometrical percentage of reinforcement.
725

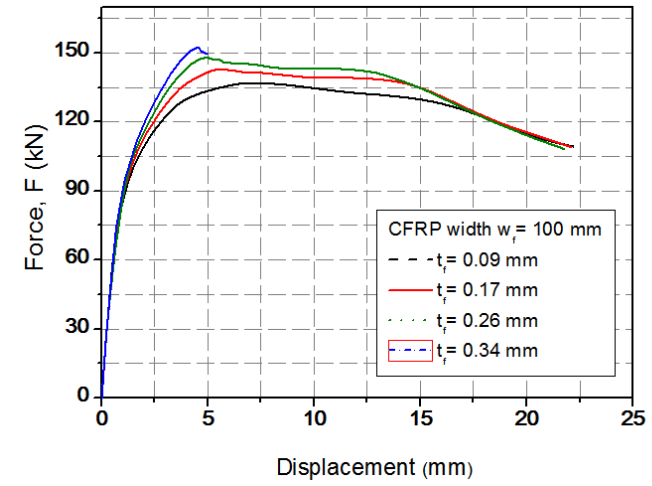

(a)

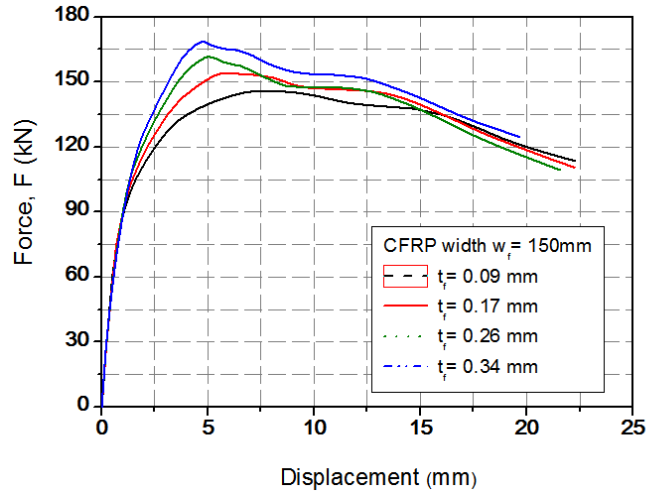

(b)

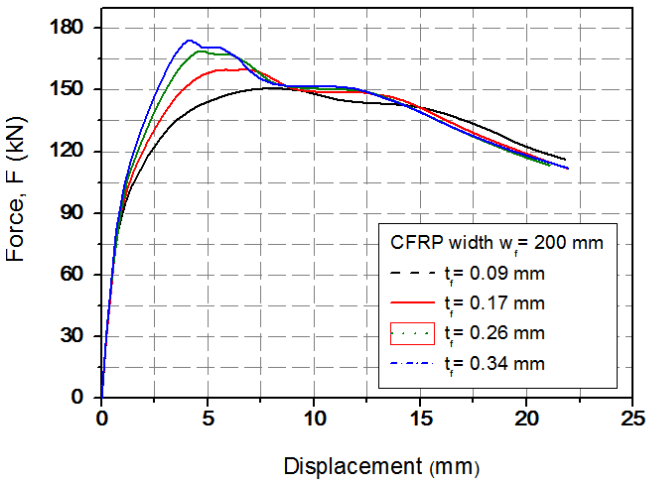

(c)

Fig. 9 Parametric study- numerical force displacemet relationship for diffrerent CFRP thickness (t_w) [0.09-0.34 mm] and width (w_f): (a) 100mm, (b) 150mm, (c) 200mm.

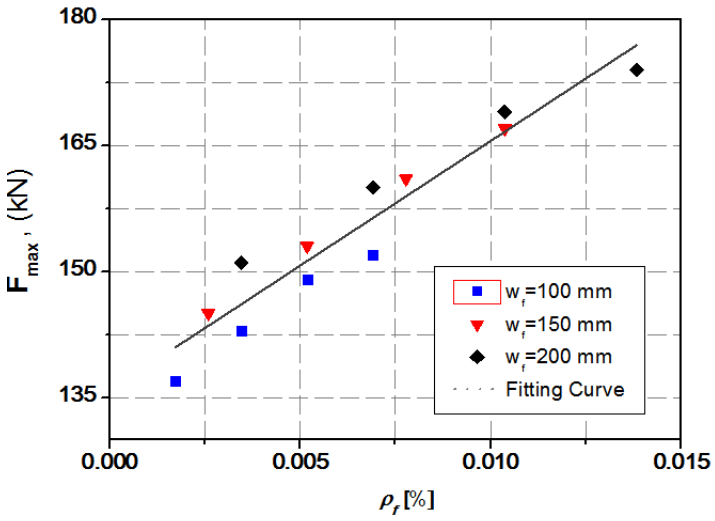

730
731 Fig. 10 Parametric study – Maximum attained load vs the percentage of CFRP strengthening.
732

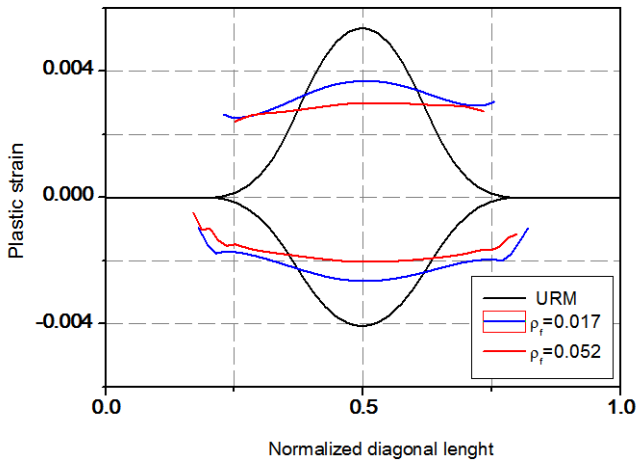

Fig. 11 Plastic strain comparison between strengthened and un-strengthened infill panel.

737

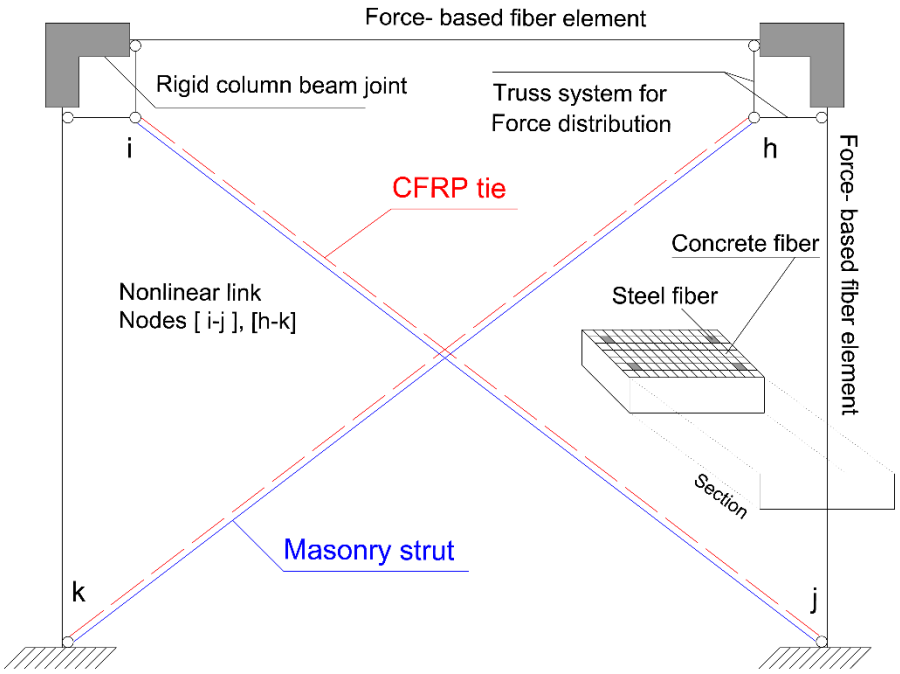

738

739 Fig. 12 Macro model of the strengthened masonry infilled frame

740

741
742

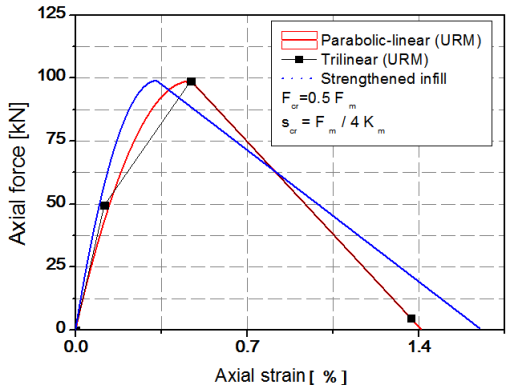

743
744 Fig.13 Strut model

745

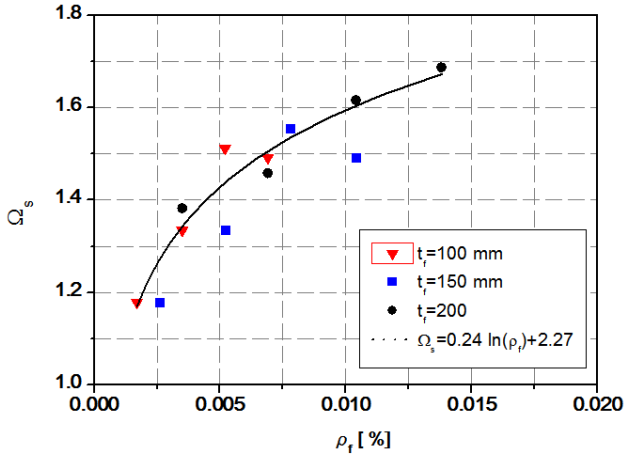

Fig 14 Ω_s vs ρ_s

751 .

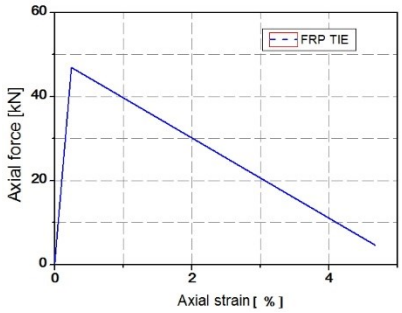

752

753 Fig 15 CFRP Tensile Tie model

754

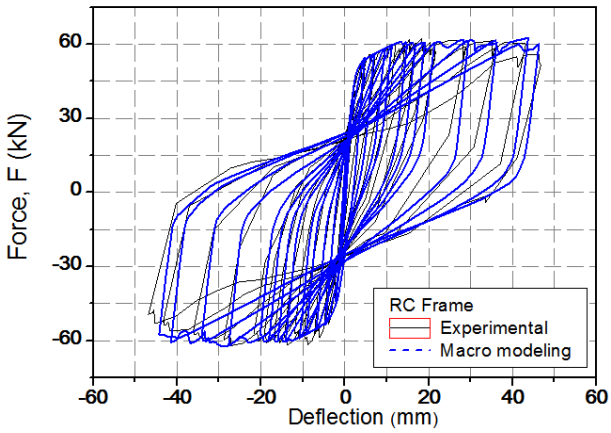

755 Fig. 16 RC Frame - experimental and macro modeling comparison

756

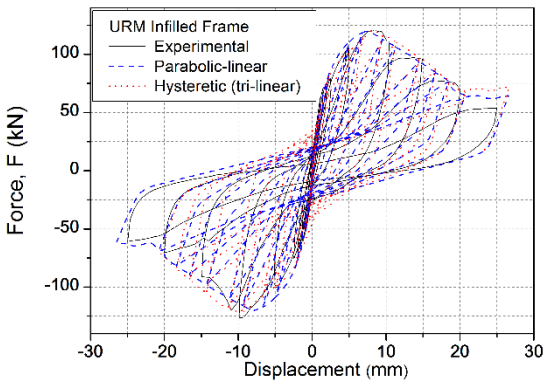

Fig. 17 URM-Infilled Frame - experimental and macro modeling comparison

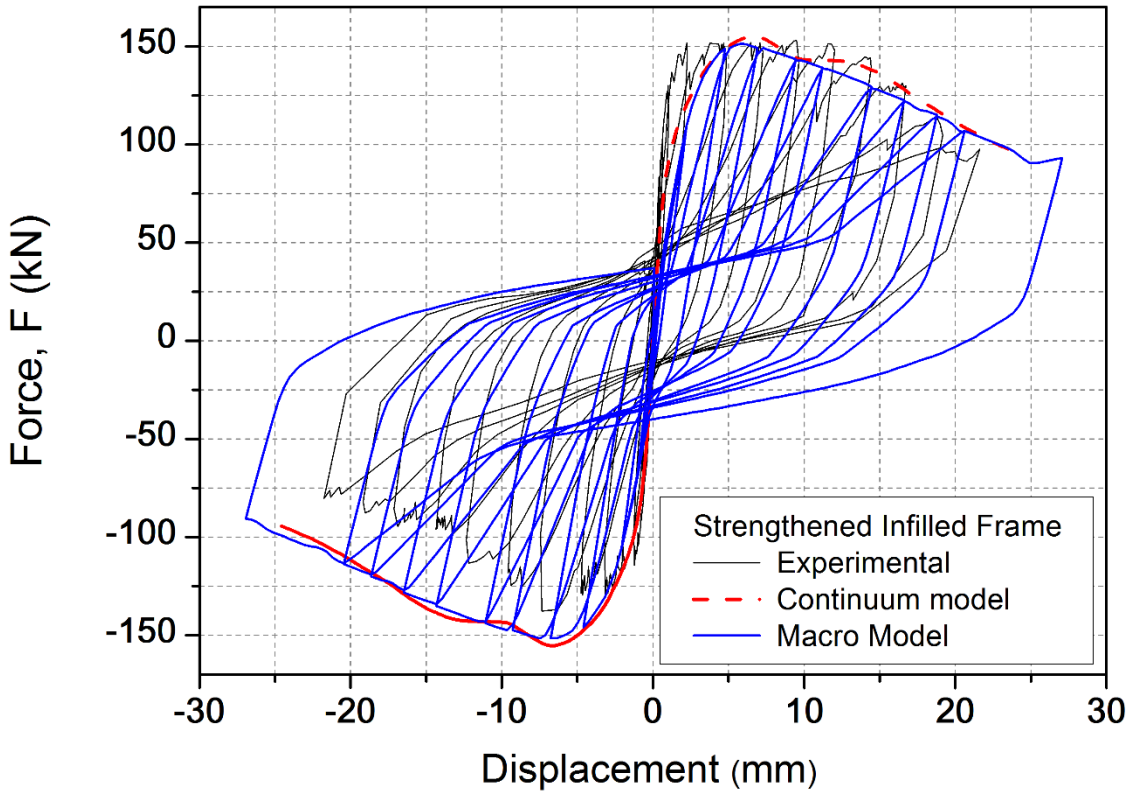

759

760 Fig. 18 Strengthened Infilled Frame – experimental, continuum and macro model comparison

761

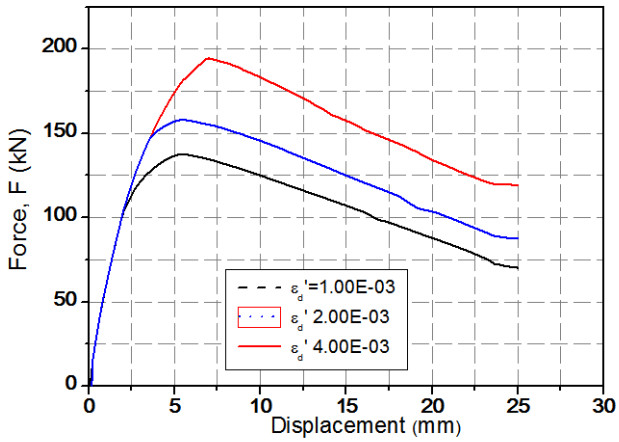

762

763 (a)

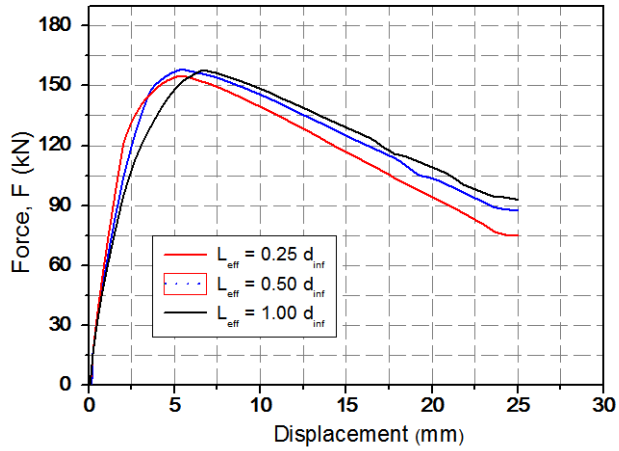

764

765 (b)

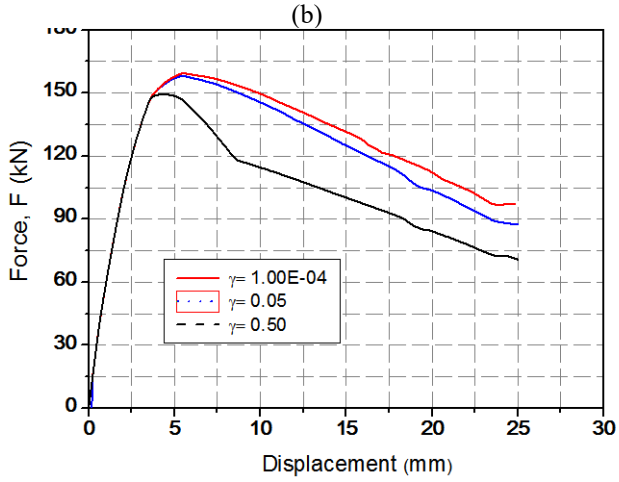

766

767 (c)

768 Fig. 19 Influence of: smeared average strain, $\varepsilon_d^{'}$ - Tie strength (a), elastic sfiffness - L_{eff} (b) and softening factor γ (c) on
769 the monotonic respone

770

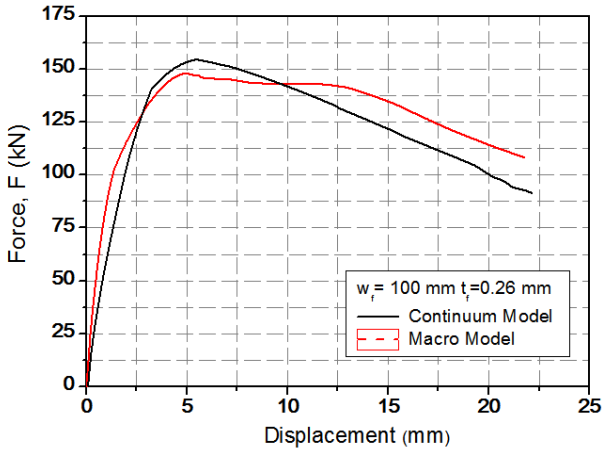

(a)

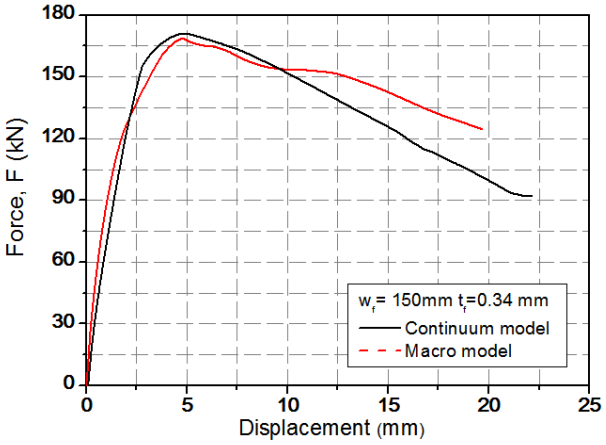

(b)

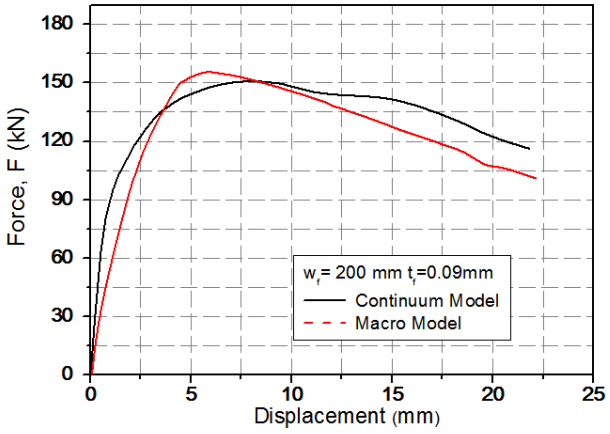

(c)

Fig. 20 Comparison between the macro model results and the parametric study (continuum modelling): (a) w_f=100mm t_f =0.260 mm (b) w_f=150mm t_f =0.340 mm (c) FRP w_f=200mm t_f =0.09 mm

Nomenclature

781

782 **Latin Letters**

A_f	CFRP area
b_w	masonry strut width in the macro modeling (URM panel)
b_w^s	masonry strut width in the continuum modeling (Strengthened panel)
b_{URM}	masonry strut width in the continuum modeling (URM panel)
d_w	masonry strut length
dL_{str}	masonry strut shortening
E	Young's modulus
E_0	masonry's Young's modulus along the direction parallel to the holes
E_{90}	masonry's Young's modulus along the direction perpendicular to the holes
E_f	CFRP Young's modulus
E_c	columns Young's modulus - concrete
E_w	masonry's Young's modulus along the diagonal
f_d	debonding stress calculated with Eq.3
f_{fdd2}	debonding stress (CNR-DT200)
f_{fdd}	intermediate debonding stress (CNR-DT200)
f_{tm}	tensile strength
f_c	compressive strength
f_w	masonry compressive stress/strength of the diagonal strut.
F_{axial}	axial force in the masonry strut
$F_{\max}$	maximum lateral force
F_{FRP}	CFRP tie force shear force – axial displacement function
$F_{FRP}^{\max}$	CFRP tie resistance
ΔF	increment of lateral force due to the CFRP strengthening
G	masonry shear modulus
G_c	fracture energy in compression
G_f	fracture energy in tension
h_w	infill panel's height
H	interstory height
I_c	moment of inertia of the column section
K_{FRP}	stiffness of the FRP tie
K_m	secant stiffness of the masonry strut
K_s	secant stiffness of the strengthened masonry strut
K_{V-d}	secant stiffness of the masonry strut in the shear – inter-story drift behavior
H	Inter-story height
l_w	infill panel's length
L	distance between the columns
L_{eff}	effective length

t_f	CFRP thickness
t_w	masonry wall thickness
$u_{\max}$	axial FRP tie displacement at peak
u_{axial}	axial FRP tie displacement
V	shear force – inter-story displacement function
V_{cr}	cracking shear strength of the infill panel
V_u	maximum shear force resistance of the infill panel
V_r	residual shear strength of the infill panel
w_f	CFRP width

783

784 **Greek Letters**

α	CNR DT200 coefficient
ξ	softening factor for the FRP model in continuum modeling
β	softening factor for the masonry strut
γ	softening factor used in the FRP tie
δ	infill panel lateral displacement
δ_{axial}	axial displacement
δ_{cr}	value of lateral displacement for V_{cr}
δ_r	value of lateral displacement for V_r
$\delta_{\max}$	axial displacement at F_{FRP}
δ_u	infill panel lateral displacement at V_u
ε_p	compressive strain at peak
ε	strain (total strain)
ε_{pl}	Plastic strain
ε_d	debonding strain calculated from f_{fdd2}
ε'_d	smeared (average) strain which identifies the maximum CFRP tie resistance
ε_{fu}	ultimate FRP strain
θ	angle of the masonry strut
θ'	angle of Infill diagonal
λ	parameter used to determinate the relative stiffness between infill and columns
σ	stress
ν	Poisson's ratio-concrete
Γ_F	fracture energy CNR-DT200
ρ_f	percentage of strengthening
Ω_s	corrective factor for the calculation of the strengthened masonry strut stiffness

785

786